

Design and Development of an Array of Dielectric Suspended Membranes for Microhotplate Applications

¹ Mahanth Prasad, ^{1,2} V. K. Khanna

¹ CSIR-Central Electronics Engineering Research Institute (CEERI) Pilani-333031 (Rajasthan), India

² Academy of Scientific & Innovative Research (AcSIR), New Delhi, India

¹ E-mail: mahanth.prasad@gmail.com

Received: 19 February 2014 /Accepted: 30 April 2014 /Published: 31 May 2014

Abstract: The paper presents the design, fabrication and characterization of an array of suspended dielectric suspended membranes for microhotplate applications. A single cell membrane ($100\ \mu\text{m} \times 100\ \mu\text{m}$) made of two different dielectric layers: SiO_2 and Si_3N_4 separately, was designed and simulated using ANSYS 10.0. The simulation of stress generated in different dielectric membranes as a function of temperature is reported. The thickness of both layers was taken as $0.3\ \mu\text{m}$. The membranes of both SiO_2 and Si_3N_4 dielectrics were fabricated on silicon substrate by bulk micromachining technique using TMAH solution. The buckling of the beam and breakage of membranes made of high-stress Si_3N_4 film are reported. The simulated results were verified by experiments. The membrane made of SiO_2 layer was found to be more suitable in comparison to high-stress Si_3N_4 layer for microhotplate applications. The present approach provides high yield at low cost for fabrication of microhotplates for gas sensing applications. Copyright © 2014 IFSA Publishing, S. L.

Keywords: Bulk micromachining, Suspended membrane, TMAH.

1. Introduction

The dielectric thin films such as SiO_2 , Si_3N_4 and combination of both are widely used in semiconductor and microelectromechanical system (MEMS) devices [1-5]. The metal oxide-based gas sensor requires elevated temperatures $250\text{-}600\ \text{°C}$ to detect the hazardous gases like carbon monoxide (CO), methane (CH_4) and ozone (O_3) etc. [6]. In microhotplate-based gas sensor, the membrane of these dielectric films is used as a platform for gas sensing [7-9]. In some cases, to reduce the stress of the membrane, the combination of both SiO_2 and Si_3N_4 layers is preferred [10-13]. Since silicon is a good heat conductor, therefore it must be removed from underneath the microhotplate membrane to achieve high thermal efficiency [14]. The removal of silicon from selected regions to form the suspended structure can be accomplished by using

bulk micromachining or surface micromachining techniques [15-17]. The thermal conductivity of gas strongly depends on the gap between the membrane and the substrate, and has a microscale effect [18]. In the present work, bulk micromachining technique was used to form the suspended structures.

Anisotropic wet etching of silicon is one of the key technologies for fabricating the microstructure and MEMS devices. The compatibility of CMOS process with MEMS fabrication is necessary for monolithic integration of analog and digital circuits to provide the signal conditioning and interface control. The chemical etchants used for fabrication of microstructure should be compatible with commercial CMOS processes because of low-cost manufacturing. The most common etchants used for anisotropic etching of Si are ethylenediamine-pyrocatechol (EDP) water, KOH, hydrazine-water (N_2H_4)_n solutions and TMAH.

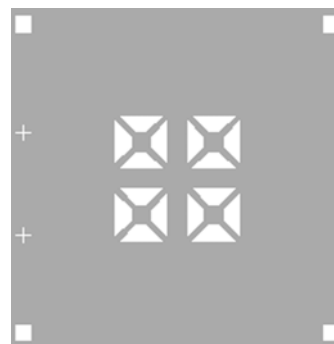
The selective etching of silicon can be done using $(\text{N}_2\text{H}_4)_n$ solutions with minimum damage to metal films. However, due to relatively high toxicity, this etchant should be handled carefully. Potassium hydroxide is an alkali metal hydroxide etchant, which has high silicon etching rate and anisotropic etching capability. But, unfortunately, it is not compatible with CMOS processing because it attacks exposed aluminum and contaminates the gate oxide with alkali mobile metal ions. The EDP solution is a diamine-based etchant, which gives anisotropic etching by adding a small amount of pyrazine. However, it is a hazardous solution with long-term toxic effects. The evaporation of EDP solution during etching is a serious inhalation hazard. Tetra methyl ammonium hydroxide (TMAH) belongs to quaternary ammonium hydroxide group, which fulfills the requirement of CMOS compatibility. It has the advantages of high etch rate, better etch characteristics, less attack on metal, and low toxicity. Nowadays, several researchers have reported the bulk micromachining of Si using tetra methyl ammonium hydroxide (TMAH) [19-25]. In the present work, the TMAH solution was used for bulk micromachining of silicon to form the suspended membrane of dielectrics layers, SiO_2 and Si_3N_4 . Many researchers have reported the different designs and fabrication processes of the dielectric membranes for microhotplates [10-13]. But, they have not presented the comparison between SiO_2 and Si_3N_4 membranes for microhotplate applications.

This paper reports the comparison of yield obtained in the fabrication of different dielectric membranes on 4-inch silicon wafers for microhotplate platform. The selection of thickness of membrane is important in the fabrication of microhotplate because it affects the operating temperature of microhotplate at an applied voltage. If the thickness of dielectric membrane is increased, then at an applied voltage, the temperature of the membrane decreases while the mechanical displacement of the membrane is reduced [26]. In order to maintain the operating temperature of the hotplate for higher thickness of membrane, more power is required. Therefore, in the present case, the membrane of $0.3 \mu\text{m}$ thickness was selected for both dielectric layers, SiO_2 and Si_3N_4 separately.

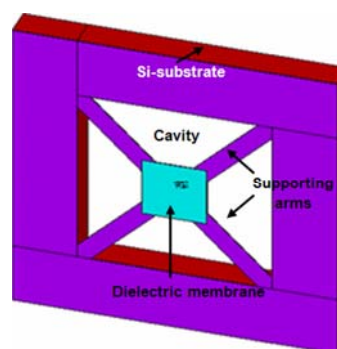
2. Design and Simulation

An array comprising four $100 \mu\text{m} \times 100 \mu\text{m}$ unit cells of dielectric membranes has been designed using L-Edit software, as shown in Fig. 1(a). The structural dimensions used in the simulation are given as follows: die size, $2.1 \text{ mm} \times 2.1 \text{ mm}$; cavity size is $300 \mu\text{m} \times 300 \mu\text{m}$ and width of the supporting arms is $30 \mu\text{m}$. The complete design consists of four trapezoidal openings to allow post-process etching of exposed silicon, forming a pit so that the membrane can be suspended in the air. There are four supporting beams for each membrane, which gives

the mechanical strength to the membrane and the connections for the heater. The single-cell dielectric membrane has the dimensions of $100 \mu\text{m} \times 100 \mu\text{m}$ over which a heater is laid out. The mechanical stress simulation of the membrane is required in order to establish the geometrical characteristics of the structure.



(a)



(b)

Fig. 1. Designed structures:
(a) layout of an array of dielectric membranes using L-Edit;
(b) unit cell membrane using ANSYS.

To verify the design, mechanical stress simulation of the unit cell of dielectric membrane has been carried out using ANSYS, widely used finite element-based software for simulation of MEMS devices. The designed structure consists of the silicon substrate over which there is a thin dielectric layer of $0.3 \mu\text{m}$ thick and a $50 \mu\text{m}$ deep cavity to form the suspended membrane [Fig. 1(b)]. In the designed unit cell, the silicon layer underlying the hotplate has been extruded to form the suspended structure. In the simulation work, SOLID69 element has been used, which supports the basic thermoelectric analysis taking joule heating effect into consideration. The SOLID69 element type has 3D thermal and electrical conduction capability. At constant applied voltage, the thickness of membrane was increased from $0.3 \mu\text{m}$ to $3 \mu\text{m}$, resulting in decrease of temperature of microhotplate [26]. This decrease in temperature is due to the heat losses to the silicon substrate layer via conduction through micro bridges. Therefore, $0.3 \mu\text{m}$ -thick dielectric membrane was chosen for analysis.

FEM mechanical stress simulation of both SiO_2 and Si_3N_4 membranes was performed by applying different temperatures (300 to 600 °C) to the membranes separately. The generated stress and displacements in the SiO_2 , and Si_3N_4 membranes have been studied separately. Standard values of physical constants and material properties used in simulation are given in Table 1. In mechanical stress simulation, a temperature of 300 °C was applied to both membranes separately. The temperature of Si substrate surrounding the membrane was fixed at 25 °C as the boundary condition.

Table 1. Material properties used in simulation.

Material	Young's modulus (GPa)	Poisson's ratio	Density (Kg/m ³)	Thermal conductivity (W/mK)	Specific Heat (J/Kg/K)
Si	150	0.17	2330	150	700
SiO_2	60	0.2	2200	1.4	1000
Si_3N_4	290	0.27	2900	3.2	170

The typical ANSYS plots of von misses stress distribution and vertical displacement in case of Si_3N_4 membrane at 300 °C is shown in Fig. 2(a).

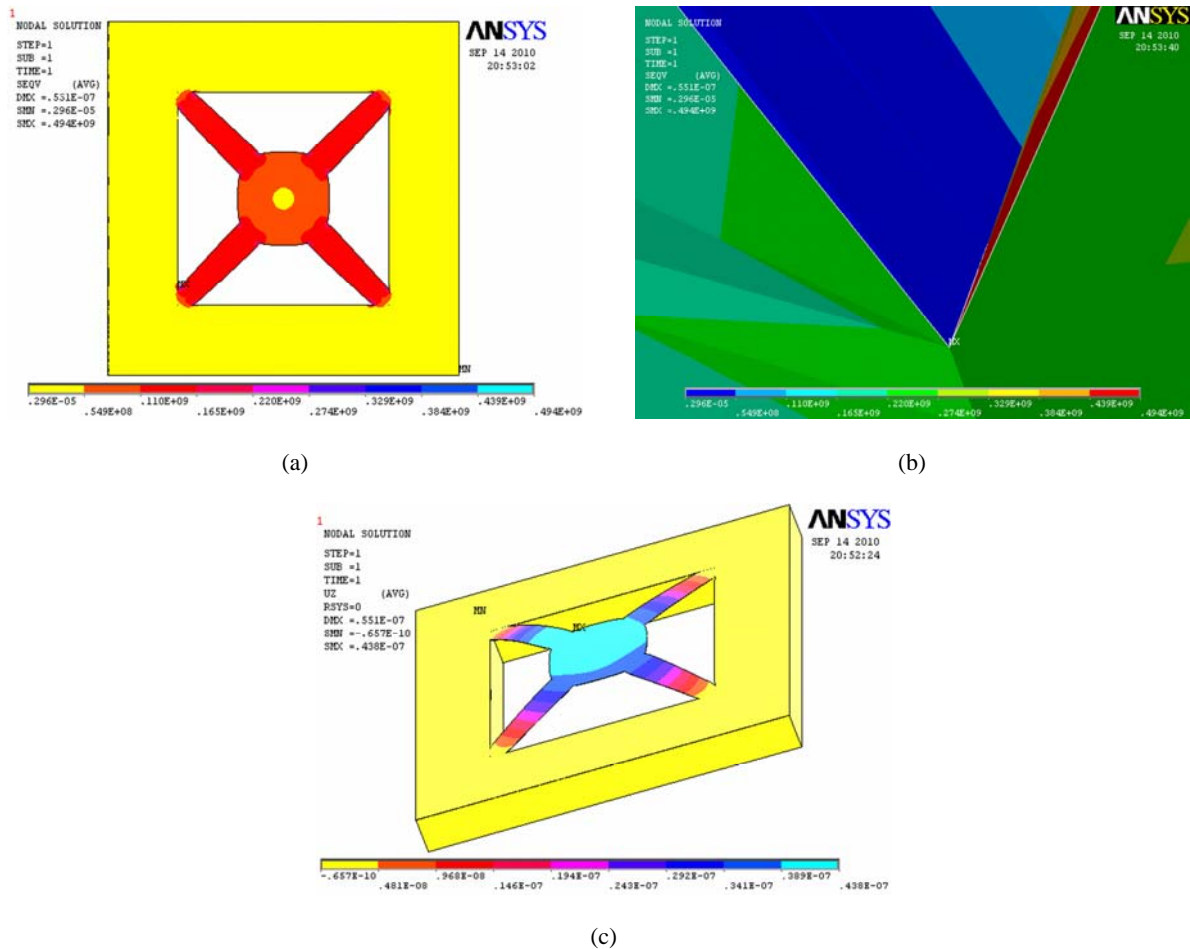


Fig. 2. FEM simulation of structures using ANSYS: (a) the mechanical von misses stress of Si_3N_4 membrane in unit cell and the surrounding regions; (b) magnified view of von misses stress distributions at edges of the arms connecting the surrounding regions; (c) vertical displacement of Si_3N_4 membrane in unit cell and the surrounding regions.

The magnified view of von misses stress distributions at the arm edge connecting the surrounding regions is shown in Fig. 2(b). It was observed that the maximum generated stress range is 439-494 MPa. Similar simulations were done by applying the different temperatures 400-600 °C in steps of 100 °C for both SiO_2 and Si_3N_4 membranes. The membrane thickness 0.3 μm was fixed in all the cases. The simulated results of temperature versus von misses stress and

temperature versus displacement for both dielectric membranes are shown in Fig. 3(a) and Fig. 3(b) respectively. It was observed from Fig. 3(a) that due to thermal effect, higher stress is generated in Si_3N_4 membrane in comparison to SiO_2 membrane. Also, it was observed that the stress linearly increases with increasing temperature in case of Si_3N_4 membrane whereas it slowly increases in case of SiO_2 membrane. Similar effects were observed in Fig. 3(b).

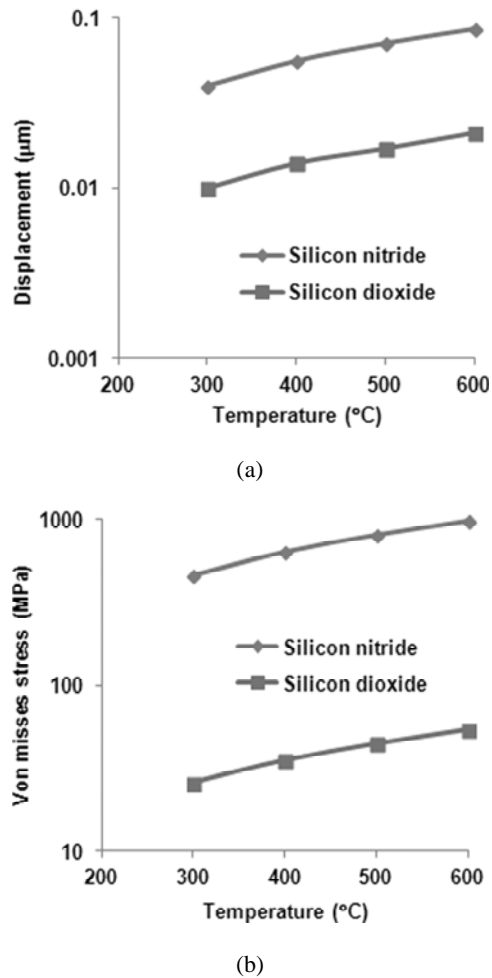


Fig. 3. FEM simulation of structures using ANSYS: (a) variation of maximum von mises stress in the dielectric membranes with increasing temperature, (b) variation of maximum vertical displacement in the dielectric membranes with increasing temperature.

3. Experimental Details and Characterization

The fabrication of micromachined structures of different membranes is started with the selection of 4-inch double sided polished P-type <100> silicon wafers. The resistivity of these wafers was 10-20 Ohm-cm. Before starting the thermal oxidation SiO_2 and low pressure chemical vapor deposition (LPCVD) process, the silicon wafers were cleaned as follows:

i) The wafers were rinsed with deionized (DI) water of resistivity 18 mega Ohm for 30 minutes to remove a large fraction of ionic impurities present on the surface except H^+ and OH^- ions.

ii) These wafers were cleaned in a heated nitric acid for 20 minutes to remove the heavy metal contaminants from the wafer surface.

iii) RCA-1 cleaning was then performed by making the solution of DI water, NH_4OH and H_2O_2 in a ratio of 5:3:3 respectively. The wafers were immersed in this solution for 30 minutes at around

80 °C temperature. This cleaning removes all organic residues and certain metal contaminants.

iv) RCA-2 cleaning was then done by making the solution of DI water, HCl and H_2O_2 in a ratio of 5:3:3 respectively. The wafers were cleaned in this solution for 30 minutes at 80 °C temperature. This cleaning removes all atomic and ionic contaminants from the wafer surface.

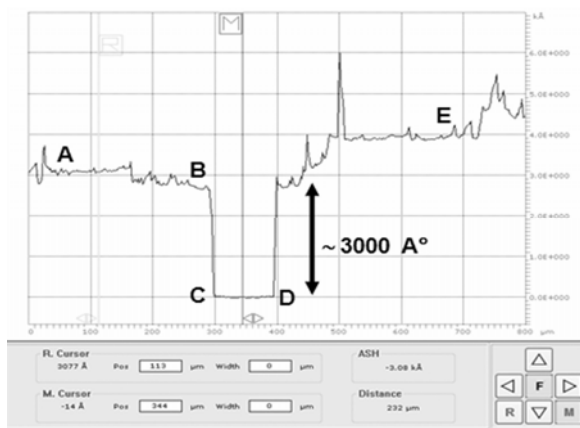
After cleaning, the wafers were dried with nitrogen gas and loaded in oxidation furnace at temperature 500 °C to avoid any crack due to rapid temperature change. In the first experiment, 0.3 µm-thick SiO_2 layer was thermally grown in a sequence of dry-wet-dry cycle at 1000 °C. Dry oxidation was performed for 10 minutes, then wet oxidation for 40 min, and again dry oxidation for 10 minutes at 1000 °C. The O_2 gas flow during dry and wet oxidation was 6 SLM (standard liters/min) and 1 SLM O_2 respectively. However, in case of wet oxidation, O_2 gas was passed through DI water was kept at 95 °C.

In the second experiment, the Si_3N_4 layer was deposited on P-type <100> silicon wafers. Before Si_3N_4 layer deposition, the wafers were cleaned similar to the cleaning steps of the first experiment. In silicon nitride deposition by LPCVD, 80 sccm (standard cubic centimeter) NH_3 and 20 sccm dichlorosilane (DCS) gases were used at 800 °C temperature. The vacuum was 270 mtorr and the deposition time was 80 min. Photolithography was done on both SiO_2 and Si_3N_4 -deposited wafers using mask#1 (for cavity opening). In this process, positive photoresist S1818 was used. The process recipe for spin coating of photoresist is given in Table 2. After coating, wafers were soft baked at 95 °C for 30 min in a temperature-controlled oven. The UV exposure of 3.5 sec was given by putting the cavity mask into MA6 Double Sided Mask Aligner. Then the photoresist was developed for 1 min in MF-312 developer. After developing, the photoresist was hard-baked at 120 °C for 30 min in a temperature-controlled oven. Both the SiO_2 and Si_3N_4 layers from the wafers were removed separately by buffered hydrofluoric acid and reactive ion etching respectively. In case of reactive ion etching of silicon nitride layer, 40 sccm SF_6 and 4 sccm O_2 were used. The vacuum during the process was 10 Pa and the power was 600 W.

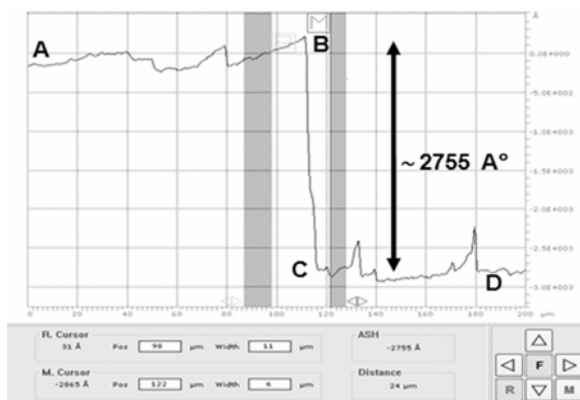
Table 2. Spinning recipe of photoresist S1818.

Process parameters	Step-1	Step-2	Step-3	Step-4	Step-5	Step-6
Speed (rpm)	0	100	2000	500	100	0
Time (sec)	4	5	20	10	10	0

After cavity opening, thickness of both dielectric layers was measured by Dektak 6M surface profiler and the plots are shown in Fig. 4(a) and Fig. 4(b) respectively.



(a)



(b)

Fig. 4. Thickness of dielectric layers measured by Dektak 6M Surface Profiler: (a) SiO₂ layer; (b) Si₃N₄ layer.

In Fig. 4(a), the stylus of the profiler moves from point A to B on silicon dioxide surface. From point B to C, it goes down towards silicon surface and then travels from point C to D on the silicon surface of the structure. It starts climbing up the silicon dioxide wall from point D to E and ends at point F. The average step height (ASH) from point B to C or D to E is measured as SiO₂ thickness and found to be 0.3 μm. Similar measurement is done in case of Si₃N₄ [Fig. 4(b)]. The average step height (ASH) from point B to C is measured as thickness of Si₃N₄ and found to be 0.27 μm. Now, anisotropic etching of silicon was performed on these wafers. In this process, 25 % TMAH solution was used. The dielectric layers SiO₂ and Si₃N₄ served as masking layers during bulk micromachining of silicon. All the experiments were carried out in a glass vessel with rotating Teflon-made boat at 4 rpm. The temperature of TMAH solution was kept constant at 65 °C by means of a temperature-controlled hotplate. The silicon etching was done for fabrication of both silicon dioxide and silicon nitride membranes. The etching time and solution temperature were kept as approximately 4 hours and 65 °C. The cavity depth was measured by Dektak 6M surface profiler, similar to Fig. 4(a). The average step height (ASH) from point B to C or D to E (Fig. 5)

was measured as cavity depth and found to be 45.0 μm. First, the silicon nitride membranes were observed by SEM. It was found that the supporting arms of the membrane were bent at the edges connecting the substrate surrounding the membrane. An array of fabricated silicon nitride membranes is shown in Fig. 6(a).

A SEM image of a single silicon nitride suspended membrane is shown in Fig. 6(b). The bended portion of the arms, supporting the membrane is encircled. The bending in the arms produces the low yield of the device and may damage the structure when microhotplate temperature increases. Also, the bending in the arms occurs due to stress generated in the film during deposition.

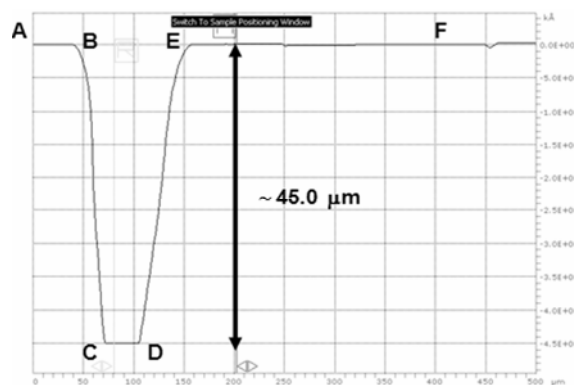
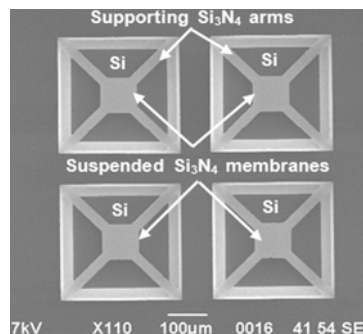
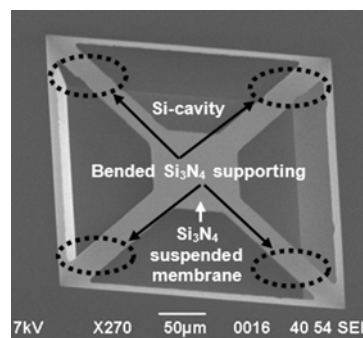


Fig. 5. Cavity depth measured by Dektak 6M surface profiler.



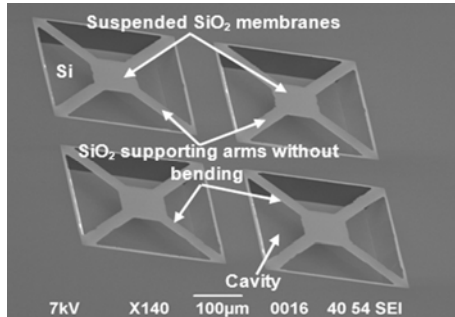
(a)



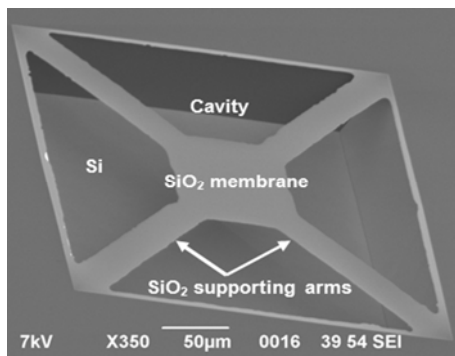
(b)

Fig. 6. SEM image of 0.3 μm-thick Si₃N₄ suspended membrane: (a) an array; (b) single membrane.

However, this defect was not observed in case of silicon dioxide membranes. The SEM photographs of an array and a single membrane of silicon dioxide are shown in Fig. 7(a) and Fig. 7(b) respectively. It was observed that the supporting arms of the membrane fabricated by silicon dioxide layer do not have any bending at the edge joining the silicon substrate.



(a)



(b)

Fig. 7. SEM image of 0.3 µm-thick SiO₂ suspended membrane: (a) an array and (b) single membrane.

It was observed that the membranes were suspended over smooth cavities and also the membranes or their supporting arms were free from bending, damages and any other defects. This gives high fabrication yield of the device in case of SiO₂-based membrane. Since the thermal diffusivity of SiO₂ is smaller than the thermal diffusivity of Si₃N₄, therefore the SiO₂ film shows better performance compared to Si₃N₄ film at higher temperatures with same power consumption, i.e., SiO₂ layer is most suitable for microhotplate platforms where high temperature operation is required at low power consumption.

4. Conclusions

The design, simulation and fabrication of an array of SiO₂ and Si₃N₄ dielectric membranes for microhotplate platform have been carried out. It is concluded that higher stress is generated in Si₃N₄ membrane as compared to SiO₂ membrane. The generated stress and deflection of both SiO₂ and

Si₃N₄ membranes were studied at different temperatures. These results give an idea about the selection of membrane materials and thickness to get the maximum yield in fabrication of microhotplate. The simulated results were compared with experimental results. The bending in supporting arms of Si₃N₄ membrane was observed, indicating high stress in the membrane. However, fabricated SiO₂ membranes are free from bending and other defects. Finally, it is concluded that the SiO₂ membranes are most suitable for microhotplate platforms in comparison to Si₃N₄ membrane.

Acknowledgements

The authors are thankful to the Director, CSIR-CEERI for encouragement and guidance.

References

- [1]. P. Ekkels, R. W. Tjerkstra, G. J. M. Krijnen, J. W. Berenschot, J. Brugger, M. C. Elwenspoek, Fabrication of functional structures on thin silicon nitride membranes, *Microelectronic Engineering*, 67-68, 2003, pp. 422-429.
- [2]. S. Z. Ali, W. I. Milne, J. W. Gardner, Tungsten-Based SOI Microhotplates for Smart Gas sensor, *Journal of Microelectromechanical System*, 17, 6, 2008, pp. 1408-1417.
- [3]. R. Hiratsuka, D. C. V. Duyn, T. Otradian, et. al., Design considerations for thermal accelerometer, *Sens. Actuators A*, 32, 1992, pp. 380-385.
- [4]. C. Rossi, T. D. Conto, D. Esteve, B. Larangot, Design, fabrication and modelling of MEMS-based microthrusters for space application, *Smart Mater. Struct.* 10, 2001, pp. 156-162.
- [5]. D. Randjelovi, A. Petropoulos, G. Kaltsas, M. Stojanovic, Z. Lazic, Z. Djuric, M. Matic, Multipurpose MEMS thermal sensor based on thermopiles, *Sensors and Actuators A*, 141, 2008, pp. 404-413.
- [6]. P. K. Clifford, D. T. Tuma, Characteristics of semiconductors gas sensors II. Transient response to temperature change, *Sens. Actuators*, 3, 1982/83, pp. 255-281.
- [7]. D. Briand, S. Heimgartner, M. A. Gretillat, B. V. Schoot, N. F. Rooij, Thermal optimization of micro-hotplates that have a silicon island, *J. Micromech. Microeng.*, 12, 2002, pp. 971-978.
- [8]. A. Y. Ahmed, J. O. Dennis, M. N. M. Saad, W. A. Talah, Design and Simulation of a High Temperature MEMS Microhotplate for Application in Trace Gas Detection, in *Proceedings of the IEEE International Conference on Semiconductor Electronics (ICSE'08)*, Johor Bahru, Malaysia, 2008, pp. 153-157.
- [9]. J. Lee, C. M. Spadaccini, E. V. Mukerjee, W. P. King, Differential Scanning Calorimeter Based on Suspended Membrane Single Crystal Silicon Microhotplate, *Journal of Microelectromechanical Systems*, 17, 6, 2008, pp. 1513-1525.
- [10]. F. T. Zhang, Z. A. Tang, J. Yu, R. C. Jin, Thermal Analysis of a Constant Temperature Pirani Gauge Based on Micro-hotplate, in *Proceedings of the 1st*

- IEEE International Conference on Nano/Micro Engineered and Molecular Systems*, Jan. 18-21, 2006, Zhuhai, China, pp. 489-490.
- [11]. J. W. Lim, D. W. Kang, D. S. Lee, J. S. Huh, | D. D. Lee, Heating power-controlled micro-gas sensor array, *Sensors and Actuators B*, 2001, pp. 139-144.
- [12]. J. C. Belmonte, J. Puigcorbe, J. Arbiol, A. Vila, J. R. Morante, N. Sabate, I. Gracia, C. Cane, High-temperature low-power performing micromachined suspended micro-hotplate for gas sensing applications, *Sensors and Actuators B*, 114, 2006, pp. 826-835.
- [13]. D. S. Lee, S. W. Ban, M. Lee, D. D. Lee, Micro Gas Sensor Array With Neural Network for Recognizing Combustible Leakage Gases, *IEEE Sensors Journal*, 5, 3, 2005, pp. 530-536.
- [14]. M. Y. Afridi, J. S. Suehle, M. E. Zaghoul, D.W. Berning, A. R. Hefner, R. E. Cavicchi, S. Semancik, C. B. Montgomery, C. J. Taylor, A Monolithic CMOS Microhotplate-Based Gas Sensor System, *IEEE Sensors Journal*, 2, 6, 2002, pp. 644-655.
- [15]. A. B. Far, F. Flitti, B. Guo, A. Bermak, A Bio-Inspired Pattern Recognition System for Tin-Oxide Gas Sensor Applications, *IEEE Sensors Journal*, 9, 6, 2009, pp. 713-721.
- [16]. D. L. D. Voe, Thermal Issues in MEMS and Microscale Systems, *IEEE Transaction on Components and Packaging Technologies*, 25, 4, 2003, pp. 576-583.
- [17]. M. Graf, D. Barrettino, M. Zimmermann, A. Hierlemann, H. Baltes, S. Hahn, N. Barsan, U. Weimar, CMOS Monolithic Metal-Oxide Sensor System Comprising a Microhotplate and Associated Circuitry, *IEEE Sensors Journal*, 4, 1, 2004, pp. 9-16.
- [18]. J. Wang, Z. Tang, J. Li, F. Zhang, A MicroPirani Pressure Sensor Based on the Tungsten Microhotplate in a Standard CMOS Process, *IEEE Transaction on Industrial Electronics*, 56, 4, 2009, pp. 1086-1091.
- [19]. J. J. Tasur, C. H. Du, C. Lee, Investigation of TMAH for front-side bulk micromachining process from manufacturing aspect, *Sensors and Actuators A*, 92, 2001, pp. 375-383.
- [20]. M. Shikida, K. Sato, K. Tokoro, D. Uchikawa, Differences in anisotropic etching properties of KOH and TMAH solutions, *Sensors and Actuators*, 80, 2000, pp. 179-188.
- [21]. P. H. Chen, H. Y. Peng, C. M. Hsies, M. K. Chyu, The characteristic behavior of TMAH water solution for anisotropic etching on both Silicon substrate and SiO₂ layer, *Sensors and Actuators A*, 93, 2001, pp. 132-137.
- [22]. P. Liebert, Encapsulation of naked dies for bulk silicon etching with TMAH, *Microelectronics Reliability*, 42, 2002, pp. 1939-1944.
- [23]. P. Papet, O. Nichiporuk, A. Kaminski, Y. Rozier, J. Kraiem, J. F. Lelievre, A. Chaumartin, A. Fave, M. Lemiti, Pyramidal texturing of silicon solar cell with TMAH chemical anisotropic etching, *Solar Energy Materials & Solar Cells*, 90, 2006, pp. 2319-2328.
- [24]. D. Cheng, M. A. Gosalvez, T. Hori, K. Sato, M. Shikida, Improvement in smoothness of anisotropically etched silicon surfaces: Effects of surfactant and TMAH concentrations, *Sensors and Actuators A*, 125, 2006, pp. 415-421.
- [25]. P. Pal, K. Sato, M. Shikida, M. A. Gosalvez, Study of corner compensating structures and fabrication of various shapes of MEMS structures in pure and surfactant added TMAH, *Sensors and Actuators A*, 154, 2009, pp. 192-203.
- [26]. J. O. Dennis, A. Yousif, M. N. Mohamad, Design Simulation and Modeling of a Micromachined High Temperature Microhotplate for Application in Trace Gas Detection, *IJET-IJNES*, 10, 02, 2010, pp. 89-96.

2014 Copyright ©, International Frequency Sensor Association (IFSA) Publishing, S. L. All rights reserved.
(<http://www.sensorsportal.com>)

Promoted by IFSA

Status of the MEMS Industry Report up to 2017

Report includes MEMS device markets, key players strategies, key industry changes and MEMS financial analysis. It also includes major MEMS manufacturing evolutions as well as an update on the "emerging" MEMS device markets.

Order online:

http://www.sensorsportal.com/HTML/Status_of_MEMS_Industry.htm